Biophysical Chemistry 140 (2009) 39–50

Contents lists available at ScienceDirect

Biophysical Chemistry

journal homepage: http://www.elsevier.com/locate/biophyschem

Theoretical examination of aggregation effect on the dielectric characteristics of spherical cellular suspension

Amit Ron [a,*], Nick Fishelson [a], Nathan Croitoriu [a], Dafna Benayahu [b], Yosi Shacham-Diamand [a]

[a] Department of Physical Electronics, Faculty of Engineering, Tel-Aviv University, Israel
[b] Department of Cell and Developmental Biology, Sackler Faculty of Medicine, Tel-Aviv University, Israel

ARTICLE INFO

Article history:
Received 11 November 2008
Accepted 16 November 2008
Available online 3 December 2008

Keywords:
Aggregation
Gap junction
Transmembrane potential
Complex permittivity
Interfacial polarization
Finite numerical analysis

ABSTRACT

Dielectric dispersion analysis of cellular suspension is generally based on the analogy to equivalent periodic material made up of identical inclusions. However, under true physiological conditions, when coupling and aggregation events usually occur, this analogy can introduce severe errors when attempting to probe the dielectric characteristics of the suspended fraction. In the framework of this study, a theoretical examination of the effect of aggregation on the dielectric characteristics of spherical cellular suspension is presented. Here, small clusters of coupled and fused (gap connected) shelled spheres were used to imitate the presence of aggregates when suspended in a homogenous suspension of spherical cells. The permittivity spectra of the aggregate-cell mixtures were numerically calculated by applying computational solution of complex potential problem using 3D Boundary Element Method. The dispersion characteristics of the mixtures have been determined as function of both aggregates shape and concentration. Those reveal significant deviations in comparison to the characteristics of homogenous cellular suspension. Quantitative analyses of the induced fields and transmembrane potential gradients of the interacted cells suggest that those deviations are mainly induced due to changes occur on the polarization state of the membranes.

1. Introduction

When cells collide, reorganization can occur in the intra as well as in the intercellular regions resulting in a stable adhesion also known as aggregation. This behaviour of cultured cells is not confined for specific type of cells and has been observed for many suspended cell lines [1–3]. The mechanism of aggregation is fundamentally based on a core of microfilaments passing through the cell membrane which have a contractile function to pull cell surfaces together upon contact [4,5]. Therefore, in most cases, undamaged membrane structures are necessary to ensure stable aggregation of cells [6].

In general, due to the destructive effect of dissociation which is often necessary in order to bring cells into suspension, aggregation can be limited to passive flocculation such as can be induced with inert particles or droplets. However, when stable aggregation is occurred, it usually involves the rapid arrangement of cytoplasmatic microfilaments which run along either side of the opposed cell membranes in parallel alignment [6]. This unique appearance, of intercellular junctions on well established aggregates, is usually formed at relatively short period of aggregation (up to few minutes) [7,8]. Those junctions, which also known as anchoring junctions, are mainly attributed to maintain cell–cell adherence by linking transmembrane proteins on adjacent cells. Another type of junctions, which usually found in more mature aggregates, is known as gap junctions. Those junctions are characterized by a localized patches where the membranes of two adjacent cells are separated by a uniform narrow gap of about 2–4 nm [6]. The intercellular exchanges of ions and small molecules through these structures have key role in many cellular and biochemical activities which allow the vital communication between the coupled cells [9].

Previous interests in study the dielectric characteristics of an ensemble of coupled cells were mainly restricted to non-thermal evoked effects which are the movement and rearrangement of cells in direct result to the presence of continues and pulsed electric fields (also known as field-induced force effects) [10,11]. On the opposing side, bio-electrical studies of native aggregation phenomena were mainly directed to ensemble of gapped cells in context of excitable cell models [12,13]. In addition, the dielectric characteristics of red blood cell aggregates (also known as rouleau formation) have been intensively explored by number of authors [14,15].

The present work aims to elaborate and explore the more fundamental effect of aggregation on the dielectric characteristics of suspended cells. In general, the dielectric characteristics of cell suspensions are mainly characterized by β dispersion mechanism which is accounted for Maxwell–Wagner effect (interfacial polarization) [16]. The suspension is considered as random composite when the complex permittivity can be calculated by considering an equivalent periodic material with identical inclusions [17]. However, in more general, when random distribution is assumed within

* Corresponding author. Tel.: +972 3 6406946; fax: +972 3 6423508.
E-mail address: amitron@eng.tau.ac.il (A. Ron).

0301-4622/$ – see front matter © 2008 Elsevier B.V. All rights reserved.
doi:10.1016/j.bpc.2008.11.008

physiological suspensions, it is normally highly irregular. Under true physiological conditions, when coupling and aggregation events usually occur, the assumptions of homogeneity and unity are no longer valid, especially when adherent cell lines are introduced [6]. At this case, the obtained dispersion characteristics will not truly represent the native behaviour of homogenous cellular suspension. This issue can introduce severe errors especially when attempting to probe the electrical properties of suspended cells based on those characteristics [18].

In this study, a theoretical examination of aggregation effect on the dielectric characteristics of spherical cellular suspension is presented. Here, small clusters of coupled and fused (gap connected) shelled spheres were used to imitate the presence of aggregates when suspended in a homogenous suspension of spherical cells. The complex permittivity spectrum of the aggregate-cell mixtures were numerically calculated using the unit cell approach [19] by applying computational solution of complex potential problem using 3D Boundary Element Method (BEM) [20]. Based on the given analysis, the dispersion characteristics of several aggregate-cell mixtures have been determined as function of aggregates shape and concentration. The obtained values indicate the wide effect of aggregation on the dielectric characteristics of cell suspensions even when low volume fraction of aggregates is introduced. This effect found to be more intense when fused aggregates are presented.

The obtained results are further elaborated by quantitative analyses of the permittivity spectrum of adjacent and coupled cells. Those indicate that electrical interactions between cells can be negligible down to separation distances of about cell diameter. In addition, the low permittivity spectrum of fused cells is found to be substantially more perturbed than those of separated and adherent cells in a given horizontal electric field. Those perturbations are found to be more moderates when the gap diameter is approaching to ~0.5% of the cell diameter. The presented findings are greatly discussed by matched analysis of the induced fields and transmembrane potential (TMP) gradients of the interacted cells.

2. Modeling of complex permittivity

The stated problem is refereed to the complex permittivity of aggregates-spherical cells mixture which is suspended in a lossy continuous medium (Fig. 1). The complex permittivity of the mixture is numerically calculated using three phase model including the suspended medium, the thin low-conducting lipid membrane, and the cytoplasm space. Each component within the described system is characterized by both relative permittivity ε' and conductivity σ when the complex relative permittivity of each component is given by:

$$\varepsilon^* = \varepsilon' - j\sigma/\omega\varepsilon_0 \quad (1)$$

where $\varepsilon_0 = 8.85 \cdot 10^{-12}$ C^2/Nm^2 is the permittivity of free space and ω is the angular frequency. Important assumption that should be taken into account is that all components (suspended medium, lipid membrane and cytoplasm space) are loss free, and also have well defined constant characteristics at the given frequency range. This assumption does not exclude the possibility that those components demonstrate dielectric loss in higher frequency range. In addition, the lipid membrane is assumed to behave as isotropic dielectric materials when the charge distribution near each interface (medium-membrane, membrane-cytoplasm) is assumed to have a null thickness, meaning absence of ionic polarization. This assumption is supported by the Debye screening length of most high conducting physiological mediums which is typically found to be quite small (typically few angstroms) in comparison to the thickness of the lipid membrane (~10 nm). It means that the electrostatic potential and the ionic double layer adjacent to the membrane have only moderate effect on the surface potential (see the extended Gouy–Chapman theory for finite size divalent cation by Alvarez et al. [21]). Therefore, the polarizability at relative low frequency (~100 Hz–1 kHz) due to counter-ion displacement can be neglected for the stated problem.

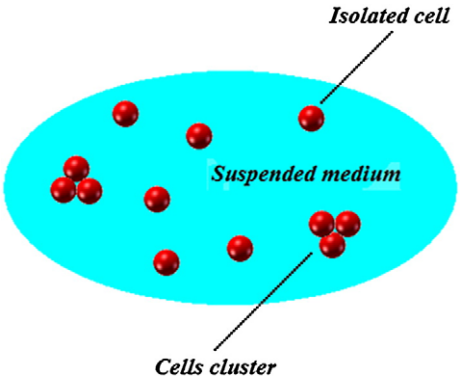

Fig. 1. Mixed dielectric model, aggregates and cells are randomly suspended in a lossy continuous medium. The complex permittivity of the mixture is determined based on three phase model including the suspended medium, the thin low-conducting lipid membrane, and the cytoplasm space. Each component is characterized by its relative permittivity ε and conductivity σ.

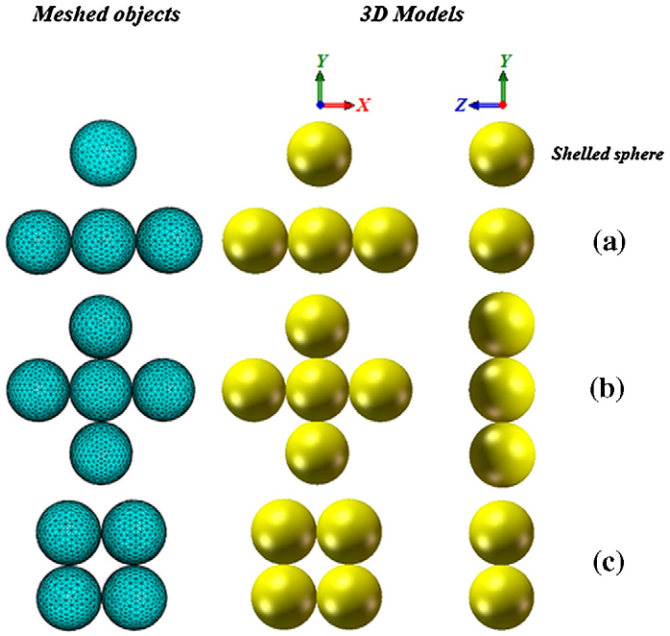

Fig. 2. Cell and aggregate models. All aggregates are composed from single shelled spherical structures. The models are precisely meshed using linear triangular elements.

2.1. Cell and aggregates models

A spherical structure consists of poorly conducting shell enclosing a conducting and polar internal core was used as a model for a biological cell. The radius of the cell was taken to be $R = 2.5$ μm with a membrane thickness of $d = 10$ nm. The dielectric phase parameters have been determined based on the average characteristics of biological cells [22] and set as follow: cytoplasm relative permittivity $\varepsilon_c' = 70$, cytoplasm conductivity $\sigma_c = 0.6$ S/m, membrane relative permittivity $\varepsilon_m' = 5$ and membrane conductivity $\sigma_m = 10^{-5}$ S/m. The characteristics of the suspended medium were taken to be $\varepsilon_{sm}' = 80$ and $\sigma_{sm} = 0.7$ S/m which stand for the relative permittivity and conductivity respectively.

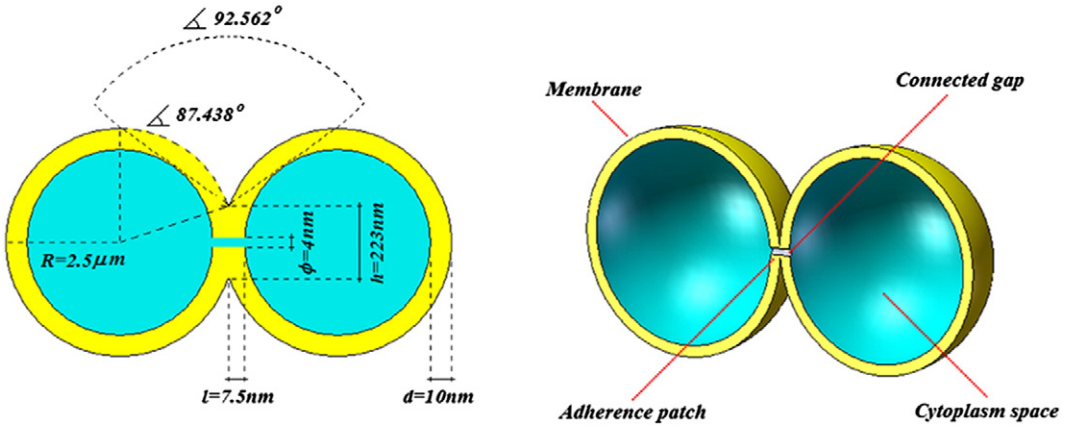

Fig. 3. 2D (left) and 3D (right) cross section models of adherent and fused cells. Adherence of cells is achieved by minimally overlapping the membranes of neighbor cells. The contact angle is defined between the contact point of the external membranes to the vertexes of the cells. When the cells are fused, an internal cylindrical channel is added which directly connects the internal cores of the cells.

Modelling of cell aggregates is fundamentally based on assembly of single shelled spherical structures into clusters of 3–5 cells (Fig. 2). Two configurations of clusters were designed (Fig. 3); the first is based on adherent cells which are connected to each other by fusion of the lipid membranes. This structure is equivalent to the case of cells connected via anchoring junctions which mainly involves linking of transmembrane proteins on adjacent cells. Adherence of neighbor cells was achieved by overlapping the corresponding membranes when the contact angle between adjacent spheres is 92.562°. This minimal overlapping is well adapted to the real case of adherent cells when adherence patches of few nanometers are usually observed [6]. The second configuration is based on clusters made of gap connected (fused) cells (Fig. 3). Each cell within the cluster is connected to its adjacent neighbours via cylindrical like gap with diameter of 4 nm. The gap allows direct connection between the internal cores (cytoplasm) of all cells within the cluster. This structure is equivalent to the case usually found in mature aggregates when cells are connected to each other via gap junctions. In this case, in order to simplify the problem, only single gap is introduced between two adjacent cells.

The dielectric phase parameters of all aggregates were set to be the same as for the single sphere model in context of both cytoplasm and membrane components. In addition, the dielectric properties of all gaps were assumed to be the same as for the cytoplasm. All models were designed and constructed using the graphical interface of SolidWorks 2007 (SolidWorks Corporation) and Rhinoceros 4.0 (Robert McNeel and Associates).

2.2. Calculation of complex permittivity

The complex permittivity for all models is directly derived based on the potential distribution within a defined lattice. In general, solution of electrostatic problem within a conducting and dielectric medium (lossy medium) is given by the continuity equation for charge which represents the complex potential of the medium.

$$\nabla \cdot (\sigma \nabla u) + \frac{\partial \rho(\bar{r})}{\partial t} = 0 \tag{2}$$

where u is the electric potential, σ represents the conductivity of the medium and $\rho(\bar{r}) = \nabla \cdot (\varepsilon \nabla u)$ represents the total charge in the considered region. For heterogeneous medium, composed of isotropic interfaces with null charge distribution and no bulk ion diffusion in all inner and outer phases:

$$\frac{\partial \rho(\bar{r})}{\partial t} = 0 \tag{3}$$

meaning no build up or depletion of charge at any point within the system. By placing Eq. (3) into Eq. (2), the governing equation for potential within the medium (using the frequency domain representation) is given by:

$$\nabla \cdot (\sigma^* \nabla u) = 0 \tag{4}$$

where σ^* is the complex conductivity defined as:

$$\sigma^* = j\omega\varepsilon_0\varepsilon^* \tag{5}$$

where $\varepsilon^* = \varepsilon' - j\varepsilon'' + \tilde{\sigma}/j\omega\varepsilon_0$ is the relative complex permittivity including the dc hopping conduction given by $\tilde{\sigma}$. In order to calculate the potential within the lattice, Eq. (4) was numerically solved using BEM (see Appendix A). A 3D cubic Lattice with single inclusion was assumed (Fig. 4). The physical boundary conditions were chosen as follows; the ground potential level was taken to be 0 V_{rms}. The excitation potential was 1 V_{rms} and the flux through the boundaries (potential derivative) was taken to be 0. The internal boundary conditions for both potential and normal displacement were given based on the structural complexity and electrical properties of the inclusion and prescribed separately on each interface within the lattice:

$$u_1 = u_2, \quad \Gamma = \Gamma_{1-2}$$

$$\varepsilon_1^* \frac{\partial u_1}{\partial n} = \varepsilon_2^* \frac{\partial u_2}{\partial n}, \quad \Gamma = \Gamma_{1-2}$$

where Γ_{1-2} is the boundary between two adjacent phases, $\partial u/\partial n$ is the component of the potential gradient in the direction normal to the

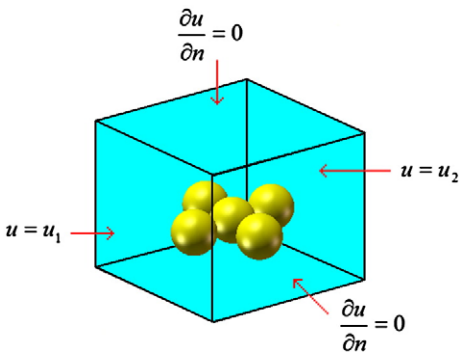

Fig. 4. 3D cubic lattice of single inclusion imbedded in continuous and conductive medium. The physical boundary conditions for both excitation potential and potential derivative are prescribed on the matched faces.

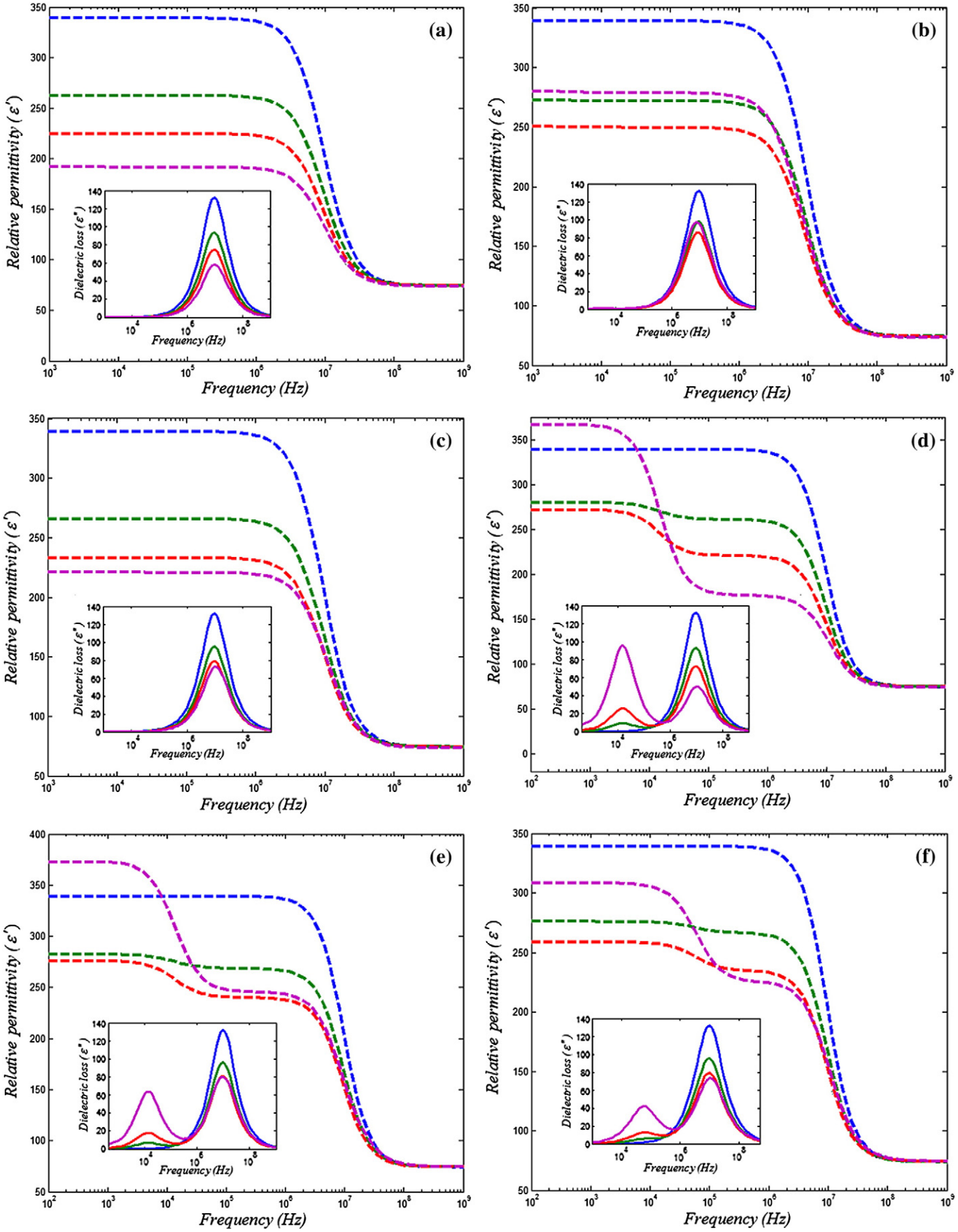

Fig. 5. Permittivity spectra of aggregate–cells mixtures. Figures a–c represent the calculated spectra of adherent aggregate mixtures and respectively referred to models A–C. Figures d–f represent the calculated spectra of fused aggregate mixtures and respectively referred to models A–C. The blue curve is referred to the spectrum of homogenous spherical suspension at volume fraction of 0.08. The red, green and pink curves represent the spectra of the mixed suspensions at aggregate–cell ratios of 1:3, 3:5 and 5:3 respectively.

surface and ε_1^*, ε_2^* are the complex relative permittivity of the two phases respectively. Calculation of potential was carried out under steady state current flow and quasistatic conditions by self-made BEM solver using MATLAB R2006a software (Mathworks Incorporation). The regions of interests were meshed using triangular linear elements for external and internal phases respectively using Abaqus 6.7 software (Dassault Systèmes). All regions were then added together utilizing continuity of fluxes (equilibrium) and equalizing the potentials (continuity) at the interfaces.

Based on Eq. (4A) (see Appendix A), the whole set of equations for all nodes of an individual subdomain can be rearranged in a matrix form when:

$$HU = GQ \tag{6}$$

where U and Q are the potential and flux raw vectors and H, G are the equivalent matrices which represent the surface integrals according to a given source node. Based on the physical boundary conditions and relation 6, all subdomains are reordered in such a way that all unknown values are found on the left hand side when:

$$[A]\overline{x} = \overline{v} \tag{7}$$

where $\overline{x}$ is the vector of unknown potential (u) and flux (q) values. The given linear system is then can be solved to extract the vector of unknown values using the successive over relaxation (SOR) iterative method [23]. See supplementary data S1 for accuracy examination of the described procedure.

Once the potential and flux values on the whole boundaries are known, the potential value at any given interior point can be calculated using Eq. (4A). After the potential is determined, the relative complex permittivity is calculated based on the total current flowing between the excited faces (hot and grounded) of the condenser. A plane, parallel to both phases is chosen. The plane is then divided to n^2 equal cubes (n rows × n columns), when the dimensions of each cube are given by: height=m, length=m, width=m; the total current flowing through the discrete plane is given by:

$$I = \sum_{j=1}^{n}\sum_{k=1}^{n} I_{j,k} = \sum_{j=1}^{n}\sum_{k=1}^{n}\left(\frac{u_{i,j,k} - u_{i+1,j,k}}{Z_{j,k}}\right) \tag{8}$$

where $u_{i,j,k}$ and $u_{i,+1,j,k}$ are the potential values across two parallel faces of the jk cube and $Z_{j,k}$ is the impedance of the jk cube given by: $Z_{j,k} = 1/j\omega m\varepsilon_0\varepsilon^*_{j,k}$. The equivalent relative complex permittivity of the cell-medium mixture can be calculated using the following equation:

$$\varepsilon^* = \varepsilon' - j(\sigma + \tilde{\sigma})/\omega\varepsilon_0 = \frac{I}{j\omega C_0 V} \tag{9}$$

where V is the applied potential between the two excited faces and C_0 is the air capacitance of the condenser. See supplementary data S2 for validation of the described procedure.

2.3. Complex permittivity of aggregates-cells mixture

The complex permittivity of given mixture is calculated by taking the statistical mean of aggregate and cell fractions within the suspended medium. This approach is equivalent to the case when random orientation of inclusions is considered [15,24]. For cells defined by complex permittivity ε_1^* and volume fraction P_1 and aggregates defined by complex permittivity ε_2^* and volume fraction P_2, the equal complex permittivity of the mixture is given by:

$$\varepsilon^* = \frac{P_1\varepsilon_1^* + P_2\varepsilon_2^*}{P} \tag{10}$$

where $P = P_1 + P_2$ is the total volume fraction of inclusions within the suspended medium.

At this case, the system is defined by diverse periodic inclusions rather than randomly distributed inclusions. This representation proved to be very useful in the case of random composite dielectric materials at relative low volume fraction of inclusions [25]. When low concentration of random distributed inclusions is introduced (~P<0.1), the complex permittivity of the suspension can be accurately simulated by considering an equivalent periodic order of inclusions. At this case, the obtained dielectric characteristics are quite similar to those obtained by modeling the true structure of the system [26].

3. Methods

3.1. Complex non linear fitting

Estimation of dispersion characteristics was performed by fitting the empirical Cole–Cole expression to the calculated permittivity spectrum. All fitted parameters were extracted based on a complex non-linear least-square fit (CNLS) which fits simultaneously both real and imaginary parts [27]; this automatically ensures that the Kramers–Kroing relations hold. The minimization function is given by Eq. (11).

$$S(\overline{P}) = \sum_{i=1}^{N} W_i^{\mathrm{Re}}\left(\varepsilon_f'(\omega_i,\overline{P}) - \varepsilon_c'\right)^2 + \sum_{i=1}^{N} W_i^{\mathrm{Im}}\left(\varepsilon_f''(\omega_i,\overline{P}) - \varepsilon_c''\right)^2 \tag{11}$$

where ε_f', ε_f'' are the fitted permittivity and permittivity loss respectively, ε_c', ε_c'' are the numerically calculated permittivity and permittivity loss respectively, N is the number of sampling points, W is the weighting factor which related to the standard deviation by $1/\sigma^2$ and $\overline{P}$ stands for the fitted parameters. The best fit parameters were determined by minimizing $S(\overline{P})$ using Levenberg–Margert algorithm [28].

4. Results

4.1. Effect of adherent aggregates

The effect of cells connected via anchoring junctions on the dielectric characteristics of spherical cellular suspension was examined by three different aggregate models (Fig. 2 models A–C). Here, aggregate-cell mixtures, at several ratios, were examined by using each of the models. The total volume fraction of all mixtures was taken to be P=0.08 when the volume ratios between the aggregates and the cells were set as 1:3, 3:5 and 5:3 respectively. The complex permittivity spectra for all models were numerically calculated using Eq. (9) within frequency range of 1 kHz up to 1 GHz using 73 sampling points. All models were assumed to orient with their longest axes parallel to the applied field, which in most cases corresponding to the minimum energy state of lossy embedded body [29]. The obtained spectra are given by Fig. 5a–c. In order to avoid confusion, the symbols A–C will also be referred to describe the three aggregate-cell mixtures respectively.

In general, all curves indicate on typical dispersion which is accounted for the Maxwell-Wagner effect (interfacial polarization) at the medium–membrane interface. The effect of aggregation on the dielectric spectrum is clearly seen in all mixtures. Both relative permittivity strength and the dielectric loss of the mixed suspensions, demonstrate significant reduction in comparison to the spectrum of homogenous spherical suspension. This tendency is observed even when low volume fraction of aggregates is introduced (P=0.02). When the volume ratio of the aggregates-cells is increased, the diminution becomes moderate for mixtures A and C when for mixture B substantial increase is observed. In addition, the characteristic frequency of mixture B is shifted to lower frequencies as the aggregates–cells ratio is increased. The opposite effect is observed for mixture C when the frequency is

slightly shifted to higher frequencies. The characteristic frequency of mixture A is not affected by the ratio differences and tends to be the same as for the spherical suspension.

In order to extract the dispersion characteristics of the spherical suspension and the mixtures, the calculated spectra were curve fitted using single Cole–Cole empirical relaxation term [30] and additional dc conductivity term:

$$\varepsilon^* = \varepsilon_h' + \frac{\Delta\varepsilon'}{1+(j\omega\tau)^{1-\alpha}} + \frac{\tilde{\sigma}}{j\omega\varepsilon_0} \tag{12}$$

here ε_h' is the limit of permittivity at high frequency, $\Delta\varepsilon'$ is the dispersion magnitude, τ is the relaxation time given by $\tau = 1/2\pi f_c$ where $f_c = 1/\tau_c$ is the characteristic frequency and α is the Cole–Cole parameter which indicates the broadness of the relaxation. All dispersion characteristics were extracted by fitting Eq. (12) to the calculated permittivity spectra using the CNLS method with weighting factor of 1, the fitted parameters are given in Table 1.

The obtained parameters indicate on the wide effect of aggregation on the dispersion characteristics of all mixtures. The permittivity strength of mixture A is greatly affected from the presence of aggregates. At high aggregates–cells ratio it is found to be 2.3 times lower in comparison to the spherical suspension. This significant reduction can be attributed to the length of the aggregate in direction parallel to the applied field. At this case, the head to tail structure seems to severely reduce the polarization of the aggregate in comparison to the one obtained by isolated cell. This effect found to be more moderate when the cross section area of the aggregate in the perpendicular direction to the field is increasing as for mixture B (1.3 times lower). At this case, the induced dipole is increasing with the spatial expending of the aggregate; therefore, the net polarization and the permittivity strength are found to be relatively higher.

The α values of mixtures B and C are found to be consistently growing as the aggregates–cells ratio is increased. This observation which is found to be quite significant for mixture B (α=0.08), indicates that the broadness of relaxation is directly affected from the presence of aggregates. This finding suggests that when the fraction of aggregates is increasing, the dispersion tend to shift towards the characteristics of the aggregates rather than of the spherical cells. It means that the "overlapping" between the two dispersion events is getting minimal. This fact is also supported by the relaxation times of mixtures B and C which found to be consistently shifted as the aggregates–cells ratio is increased. Since the relaxation time of mixture A, for all aggregate–cell ratios, found to be the same as for the spherical suspension, it can be assumed that the relaxation broadness is governed by the widthwise structure of the aggregate rather than its longitudinal structure.

4.2. Effect of fused aggregates

The effect of cells connected via gap junctions (fused cells) was examined using the models A–C given by Fig. 2. Here, each cell within the like gap with diameter of 4 nm. The total volume fraction of all mixtures and the ratios between the aggregates and the cells were taken to be the same as for the adherent aggregates analysis (Section 4.1). The complex permittivity spectra for all models were numerically calculated using Eq. (9) within frequency range of 100 Hz up to 1 GHz using 85 sampling points. All models were assumed to orient with their longest axes parallel to the applied field. The calculated spectra are given by Fig. 5d–f.

Table 1
Cole–Cole dispersion characteristics of adherent aggregate mixtures

Mixture	ε_h'	$\Delta\varepsilon'$	τ_c (μs)	α	$\tilde{\sigma}$ (S/m)
Shelled sphere, P=0.08	74	265	0.104	0	0.512
A, P=0.02	74	188	0.104	0	0.569
B, P=0.02	74.2	198	0.108	0.01	0.564
C, P=0.02	74.4	191	0.105	0	0.565
A, P=0.03	74	150	0.104	0	0.594
B, P=0.03	74.2	176	0.12	0.04	0.581
C, P=0.03	74.4	159	0.104	0.01	0.586
A, P=0.05	74	117	0.104	0	0.61
B, P=0.05	74.2	207	0.135	0.08	0.562
C, P=0.05	74.4	147	0.096	0.02	0.577

The symbols A–C are refereed to the three aggregate–cell mixtures respectively. The symbol P is referred to the relative volume fraction of the aggregates.

Table 2
Cole–Cole dispersion characteristics of fused aggregate mixtures

Mixture	ε_h'	$\Delta\varepsilon_l'$	τ_{cl} (μs)	α	$\Delta\varepsilon_h'$	τ_{ch} (μs))	β	$\tilde{\sigma}$ (S/m)
A, P=0.02	74	18	65.1	0	187	0.104	0	0.569
B, P=0.02	74.2	12	70.7	0	196	0.108	0.01	0.564
C, P=0.02	74.4	10	16.1	0	192	0.105	0	0.565
A, P=0.03	74	51	65.1	0	147	0.104	0	0.594
B, P=0.03	74.2	36	70.7	0	166	0.12	0.04	0.581
C, P=0.03	74.4	23	16.1	0	161	0.104	0.01	0.586
A, P=0.05	74	190	65.1	0	103	0.102	0	0.61
B, P=0.05	74.2	128	70.7	0	171	0.128	0.1	0.562
C, P=0.05	74.4	84	16.1	0	150	0.096	0.03	0.576

The symbols A–C are refereed to the three aggregate–cell mixtures respectively. The symbol P is referred to the relative volume fraction of the aggregates.

The obtained permittivity spectra, for all mixtures, indicate on the presence of two dispersion events. The high dispersion spectra of all mixtures are found to be in full matching with those obtained for the adherent aggregates mixtures. This fact indicates that the high dispersion event is fully governed by the interfacial polarization at the medium–membrane interface. The low dispersion event, which was not observed by the adherent aggregate models, is therefore attributed to polarization which arises due to the internal connected channels. The permittivity strength of the low dispersion is consistency growing as the aggregates–cells ratio is increased. This phenomenon is greatly observed for mixtures A and B when at high aggregates–cells ratio (5:3) it even exceeds the permittivity strength of the spherical suspension. On the other hand, based on the permittivity loss spectra, the low characteristic frequency, for all mixtures, are not affected from the change in aggregates–cells ratio. The characteristic frequency of mixtures A and B is found to be quite similar (~10 kHz) when for mixture C it is found to be significantly higher (~60 kHz).

The dispersion characteristics of the mixtures were extracted using two Cole–Cole relaxation terms and additional dc conductivity term:

$$\varepsilon^* = \varepsilon_h' + \frac{\Delta\varepsilon_l'}{1+(j\omega\tau_l)^{1-\alpha}} + \frac{\Delta\varepsilon_h'}{1+(j\omega\tau_h)^{1-\beta}} + \frac{\tilde{\sigma}}{j\omega\varepsilon_0} \tag{13}$$

where l and h are referred to the low and high dispersions respectively, and α, β are the Cole–Cole parameters which represent the relaxation broadness at low and high frequency respectively. All dispersion characteristics were extracted by fitting Eq. (13) to the calculated permittivity spectra using the CNLS method with weighting factor of 1, the fitted parameters are given in Table 2.

According to the obtained parameters, the high frequency characteristics reveal only minute deviations in comparison to the adherent aggregate mixtures. Both the dispersion frequencies, and broadness, are found to be quite similar between the two models, the permittivity strength however is found to be a bit lower in the case of the fused aggregates. The effect of the internal junctions is particularly distinguished by the low dispersion characteristics of the mixtures. The low permittivity strength, which is directly dependent on the aggregates–cells ratio, is also found to be affected by the length to width ratio of the aggregates. This affect is clearly observed by mixture A (length:width=3:1) when the permittivity strength is found to be two times higher in comparison to mixture C (length:width=1:1). It therefore can be suggested that in the case of fused aggregates, the longitudinal head to tail structure significantly increases the

polarization within the aggregate as opposed to the case of adherent aggregate when the polarization decreases.

The α values for all mixtures is found to be zero, it means that the low dispersion event can be described by classic Debye relaxation term. The relaxation times of mixtures A (τ_{cl}=65.1 μs) and B (τ_{cl}=70.7 μs), are found to be quite similar. Those however are found to be relatively higher in comparison to the relaxation time obtained for mixture C (τ_{cl}=16.1 μs). This difference can be attributed to the presence of two parallel longitudinal channels which practically increasing the effective conductance G between the two cores of aggregate C. Using the parallel R–C (resistor–capacitor) analog representation of the channel [9], it can be clearly proved that while the conductance is increasing, the relaxation time given by $\tau=RC=C/G$ is decreasing as expected.

4.3. Adhering effect

In order to quantify the adhering effect of cells, the electric interaction between pair of shelled spheres has been examined. Two configurations, corresponded to the parallel and perpendicular orientations of the cells in respect to the external electric field, were examined (Fig. 6). The geometrical and electrical properties of the cells were taken to be the same as for the unit spherical cell described at Section 2.1. The complex permittivity spectra for both orientations were numerically calculated by consistently varying the separation distance (sd) between the cells. The dielectric phase parameters for both configurations have been determined by fitting Eq. (12) to the matched permittivity spectra. The obtained permittivity spectra are given by Fig. 7a (parallel orientation) and 7b (perpendicular orientation), the dielectric phase parameters are summarized in Table 3.

As the cells approach each other, changes are observed in both the permittivity strength and the characteristic frequency for both orientations. In the parallel orientation, moderate decrement is observed in the permittivity strength while the relaxation frequency slightly increases. The opposite effect is observed for the perpendicular orientation when the permittivity strength increases while the relaxation frequency decreases. Those differences are attributed to the interaction between the induced dipoles of the interacting cells. In the parallel orientation, the two dipoles tend to shield each other throughout the approaching

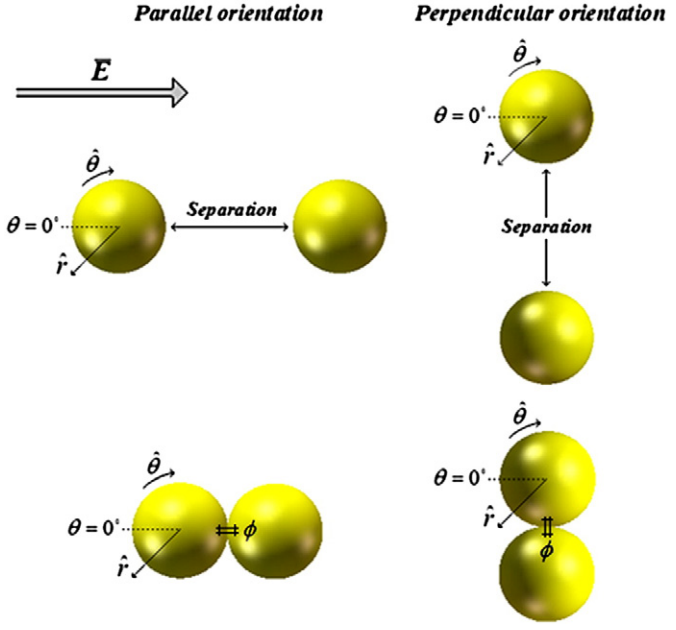

Fig. 6. Adhering (upper view) and fused cell (lower view) models. Two configurations which accounted to the parallel and perpendicular orientations of the models in respect to the external electric field are presented. The geometrical end electrical properties were taken to be the same as for the models described by Section 2.1.

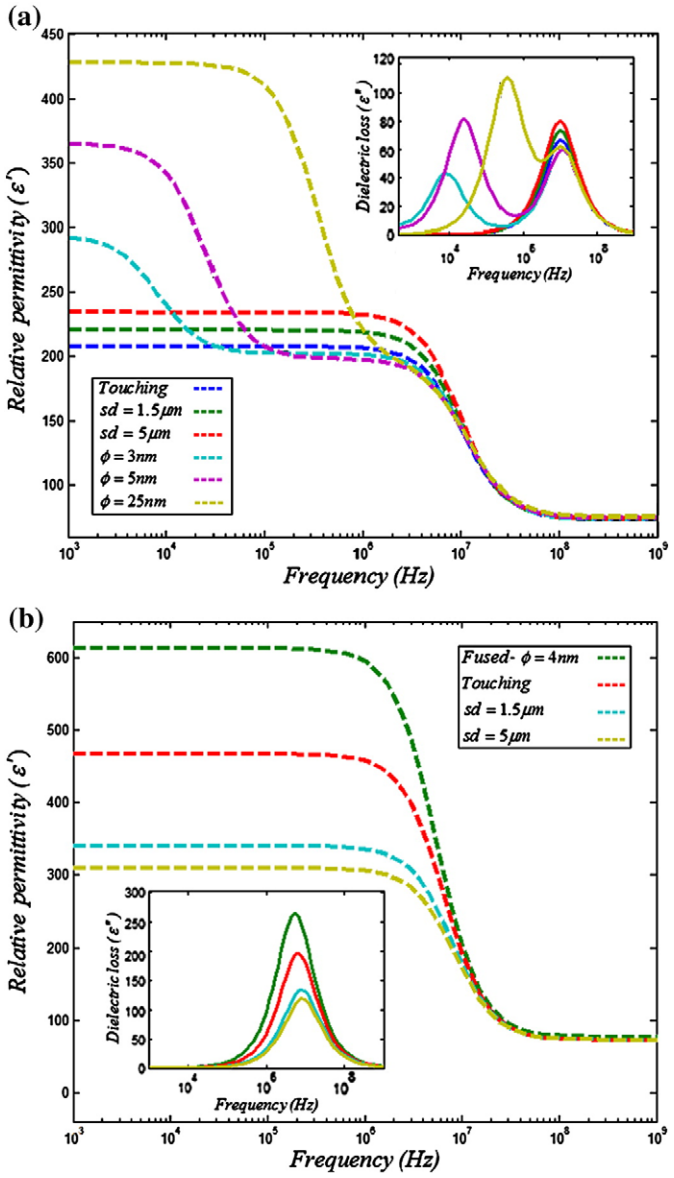

Fig. 7. Permittivity spectra of adhering and fused cells. (a) Permittivity spectra of adhering and fused cells in the parallel orientation as function of separation distance (sd) and gap diameter (ϕ). (b) Permittivity spectra of adhering and fused cells in the perpendicular orientation as function of separation distance (sd) and gap diameter (ϕ).

lane. Therefore, the net polarizability, and hence the relative permittivity, found to be constantly fading. On the other hand, in the perpendicular orientation, the dipoles are parallel aligned to each other; therefore, the electrical interaction is quite negligible. However, as the two cells approaching each other, the net contribution of the dipoles is constantly growing; therefore, the net polarizability, and hence the relative permittivity found to be higher.

The above phenomenon is well described using exponential decay function:

$$\Delta\varepsilon' = \Delta\varepsilon'(x>>\lambda) + Ce^{-x/\lambda} \tag{14}$$

where x is the separation distance between the cells, C is a constant and λ is the electrical space constant which is a function of the geometrical and electrical properties of the cell [12]. In order to extract the λ values for the two models, the relative permittivity values were curve fitted using Eq. (14). The fitted curves for both orientations are given by Fig. 8a.

Table 3
Cole–Cole dispersion characteristics of adhering cells as function of separation distance (sd)

Orientation	*Model*	ε_h'	$\Delta\varepsilon'$	τ_c (μs)	α	$\tilde{\sigma}$ (S/m)
Parallel	Touching	74	130	0.092	0	0.59
Parallel	sd=1.5 μm	74	144	0.093	0	0.586
Parallel	sd=5 μm	75	157	0.098	0	0.581
Perpendicular	Touching	73.5	395	0.15	0	0.522
Perpendicular	sd=1.5 μm	73.5	268	0.124	0	0.549
Perpendicular	sd=5 μm	73.5	237	0.119	0	0.558

The obtained values, λ=2.3 μm (parallel orientation) and λ=1.5 μm (perpendicular orientation) can provide unique insights about the nature of interaction between the cells [12,13]. In the context of this study, those allow to get a reliable estimation regarding the boundaries of interactions between spherical cells. Based on the given analysis, the electrical interactions between homogenous spherical cells are limited up to separation distance of about the cell diameter (~5 μm in the current study). Those interactions are found to be quite intense when the separation distance is getting smaller than λ ($x<\lambda$), especially in the perpendicular orientation when the permittivity strength is found to be ~1.5 times higher than normal as the cells are touching each other. When the distance is increasing, such as it exceeds the electrical space constant of the cell ($x>\lambda$), the interactions are getting weaker and the dispersion characteristics are getting fixed. In this case, the obtained permittivity spectrum will truly represent the behaviour of a homogenous cellular suspension rather than the contribution of cellular interactions.

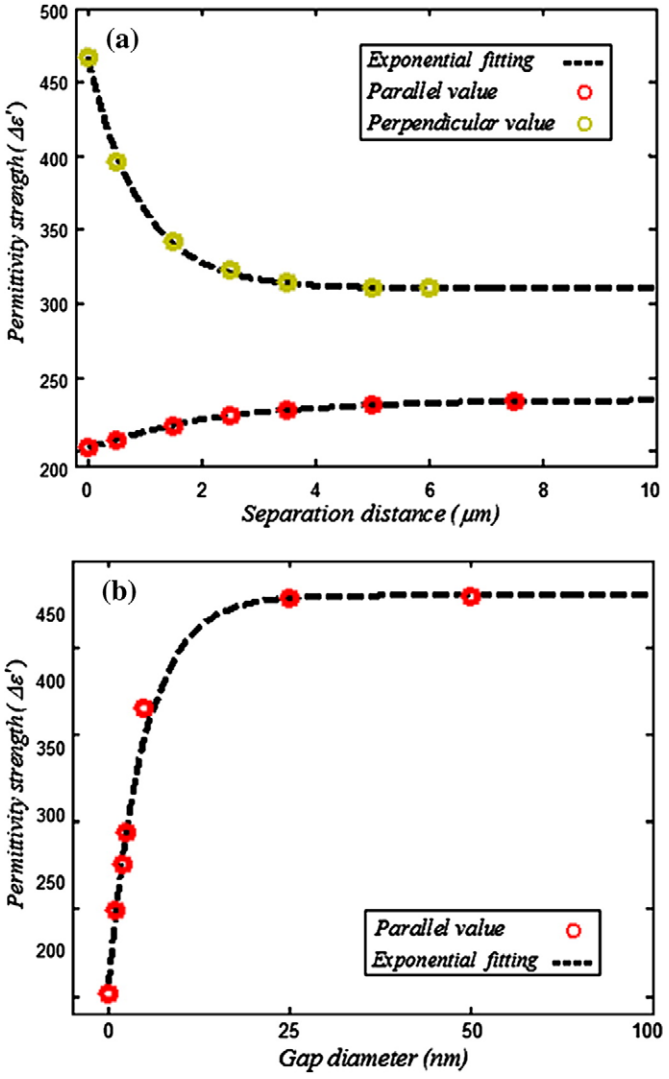

Fig. 8. Exponential fitting (black dashed line) of relative permittivity strengths (colored circles). (a) Relative permittivity strengths of adhering cells in the parallel and perpendicular orientations as function of separation distance. The fitting parameters for the parallel orientation are: $\Delta\varepsilon'(x>>\lambda)=235$, $C=-32.5$ and $\lambda=2.3$ μm. The fitting parameters for the perpendicular orientation are: $\Delta\varepsilon'(x>>\lambda)=309$, $C=158$ and $\lambda=1.5$ μm. (b) Relative permittivity strengths of fused cells in the parallel orientation as function of gap diameter. The fitting parameters are: $\Delta\varepsilon'(\phi>>\lambda)=431$, $D=-227$ and $\delta=12$ nm.

4.4. Effect of gap diameter

The effect of gap size on the dielectric characteristics of fused aggregates have been examined more closely using a fused pair of shelled spheres. The given models (Fig. 6) have been analyzed using both the parallel and perpendicular orientations. The geometrical and electrical properties of the aggregate were taken to be the same as for the fused cells model described at Section 2.1. The complex permittivity spectra for both orientations were numerically calculated by consistently varying the gap diameter ϕ between the two cores of the aggregate. The dielectric phase parameters for both configurations have been determined by fitting Eq. (13) to the matched permittivity spectra. The obtained permittivity spectra are given by Fig. 7a (parallel orientation) and 7b (perpendicular orientation), the dielectric phase parameters are summarized in Table 4.

As the gap diameter increases, significant changes are observed in the spectra corresponded to the parallel orientation. Both the low permittivity strength ($\Delta\varepsilon_1$) and the low relaxation frequency (f_l) are found to consistently growing. Those changes directly result from the reduction occurred in the gap resistivity. As the gap cross section area is increased, the conductance between the two cores of the aggregate is increasing. At this case, the voltage drop across the longitudinal patch of the aggregate causes its two poles to become more hyperpolarized and depolarized respectively. Therefore, the net polarizability, and hence the relative permittivity are found to be higher. In addition, the relaxation frequency which directly governed by the gap resistivity, is shifted to higher frequencies as expected.

The deviations in the low permittivity magnitude are well described using exponential decay function:

$$\Delta\varepsilon_l' = \Delta\varepsilon_l\{\phi>>\delta) + De^{-\phi/\delta} \quad (15)$$

where ϕ is the gap diameter, D is a constant and δ is the electrical space constant of the gap which is a function of its geometrical and electrical properties. In order to extract the δ value, the relative permittivity values were curve fitted using Eq. (15), the fitted curve is given by Fig. 8b.

Based on the given analysis, δ value of 12 nm was obtained when the effect of gap size is noticeable up to diameters of about ~0.5% of the cell diameter (~25 nm in the current study). When the diameter is smaller than δ ($\phi<\delta$), the permittivity strength is steeply rising as the gap diameter is increased. When the diameter is increased, such as it exceeds the electrical space constant ($\phi>\delta$), the effect getting weaker and the permittivity magnitude is nearly achieving its plato phase. In this case, the low permittivity spectrum is nearly constant when only small deviations are noticed on the characteristic frequency.

Table 4
Cole–Cole dispersion characteristics of fused cells as function of gap diameter (ϕ)

Orientation	*Model*	ε_h'	$\Delta\varepsilon_l'$	τ_{cl} (μs)	α	$\Delta\varepsilon_h'$	τ_{ch} (μs)	β	$\tilde{\sigma}$ (S/m)
Parallel	ϕ=3 nm	73	91	120.3	0	129	0.087	0	0.633
Parallel	ϕ=5 nm	74	167	40.5	0	124	0.087	0	0.633
Parallel	ϕ=25 nm	75	237	2.8	0	115	0.094	0.01	0.633
Perpendicular	ϕ=4 nm	75	–	–	–	537	0.185	0	0.499
Perpendicular	ϕ=25 nm	75	–	–	–	536	0.185	0	0.499

As opposed to the parallel model, on the perpendicular orientation, only minute deviations are observed between the adherent state (overlapped cells when $\phi=0$) and the fused state. At this case, changing the gap diameter has no effect on the dielectric spectrum and characteristics of the suspended aggregate. Since the dipoles are parallel aligned to each other, the gap diameter does not disturb the potential and current distributions within the aggregate. At this case, the polarizability is only governed by the separation distance between the two cores of the aggregate. Hence, the relative permittivity and the characteristic frequency are not affected.

5. Discussion

Following the presented analyses, the aggregation effect is mainly governed by the aggregate structure and its orientation in respect to the applied field. In general, adherent aggregates will normally reduce the permittivity magnitude of homogenous spherical suspension especially when long head to tail structures are formed in direction parallel to the applied field. On the other hand, fused aggregates will usually modify the spectrum by contributing additional dispersion event which is accounted for the internal connected gaps. At this case, both gap diameter, and the length to width ratio of the aggregate, will determine the relative influence of the aggregates on the obtained permittivity spectrum.

From realistic point of view, the analysis of complex aggregate–cell mixtures can be quite complicated. Therefore, in order to gain useful realizations about the aggregation effect, the nature of interactions between adherent and fused cells has been analyzed using simple model as given in Sections 4.3 and 4.4. Those models allow evaluating the general deviations obtained on both the dielectric spectrum and characteristics in response to cell aggregation. Based on those models, the induced polarization within adherent cells is found to be reduced in the parallel orientation and enhanced in the perpendicular orientation. This effect is found to be much significant when the distance between the cells is getting smaller than the electrical space constant λ. When the cells are fused (gap connected), significant effect is mainly observed at the parallel orientation when the polarization is greatly increasing. At this case, the low permittivity magnitude found to be consistently growing as the gap diameter increased. This exponential increment slowly fades as the gap diameter is getting higher than the electrical space constant of the gap δ.

In order to quantify the electrical effect of aggregation, the transmembrane potential (TMP) and the induced membrane fields of adherent and fused cells have been analyzed. The TMP represents the electrical potential difference between the interior and exterior of the cell; therefore, it can greatly reflect changes on the electric polarization in response to interaction between cells [13,15]. Using the two models given by Fig. 6, the TMP and the tangential membrane field have been analyzed for both the parallel and perpendicular orientations. The TMP gradients versus the azimuthal angle θ are given by Fig. 9. The membrane field strengths are given by Fig. 10. All curves were numerically computed at frequency of 100 Hz which is well below the low dispersion frequency of the models.

As for the parallel orientation, when the cells approach each other, the TMP gradient shifts progressively (Fig. 9a). The right pole of the cell is getting more depolarized while its left pole tends to remain under constant gradient. Those changes reflect the tendency of the cells to shield each other near the point of contact as they become close to each other. Therefore, both polarization and the permittivity strength are getting lower. When the cells are fused, the two poles become more hyperpolarized and depolarized as the gap diameter is increased (Fig. 9a). When the gap diameter is exceeding the electrical space constant δ, the TMP clearly vanishes near the point of fusion ($160 \le \theta \le 180$). This indicates that at this point the polarization within the aggregate reached its maximal strength. The obtained field curves (Fig. 10a) are in full agreement with the

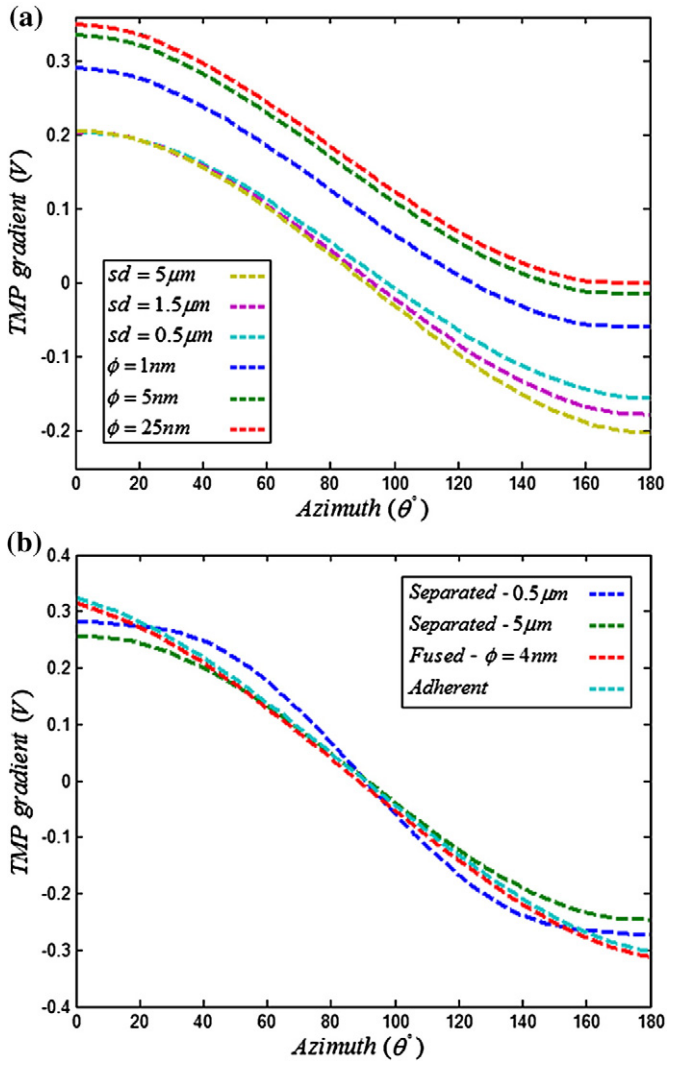

Fig. 9. Transmembrane potential (TMP) gradients versus the azimuthal angle θ of adhering and fused cells. (a) TMP gradients of adhering and fused cells in the parallel orientation as function of separation distance (sd) and gap diameter (ϕ). (b) TMP gradients of adhering and fused cells in the perpendicular orientation as function of separation distance (sd) and gap diameter (ϕ).

calculated TMP curves. During the approach phase, the field strength is gradually decreasing near the approaching point resulting in depolarization of the membrane. When the cells are in full contact, the depolarization is getting more intense when the field in close proximity to the adhering patch found to be totally fading.

As opposed to the parallel orientation, in the perpendicular orientation the TMP amplitude found to be consistently increasing as the cells approach each other (Fig. 9b). It means that both poles of the cell are getting more hyperpolarized. When the cells are fully adhering, the hyperpolarization is found to be higher when the TMP curve is getting smoother. This indicates that at this point the polarization is fully generated by the contribution of the two dipoles as in a single continuous structure. When the cells are fused, only minor deviations are observed on the TMP curve, this indicates that the contribution of the gap to the net polarization is quite insignificant at the perpendicular orientation. The simulated field curves (Fig. 10b) are found to be well adapted to the tendency observed by the TMP curves. As the hyperpolarization increases, the membrane field strength found to be higher as expected. At this case, the field strength represents the additive contribution of the two parallel dipoles which found to be maximal as the cells are in full contact. When the cells are fused, only minute deviations are observed in

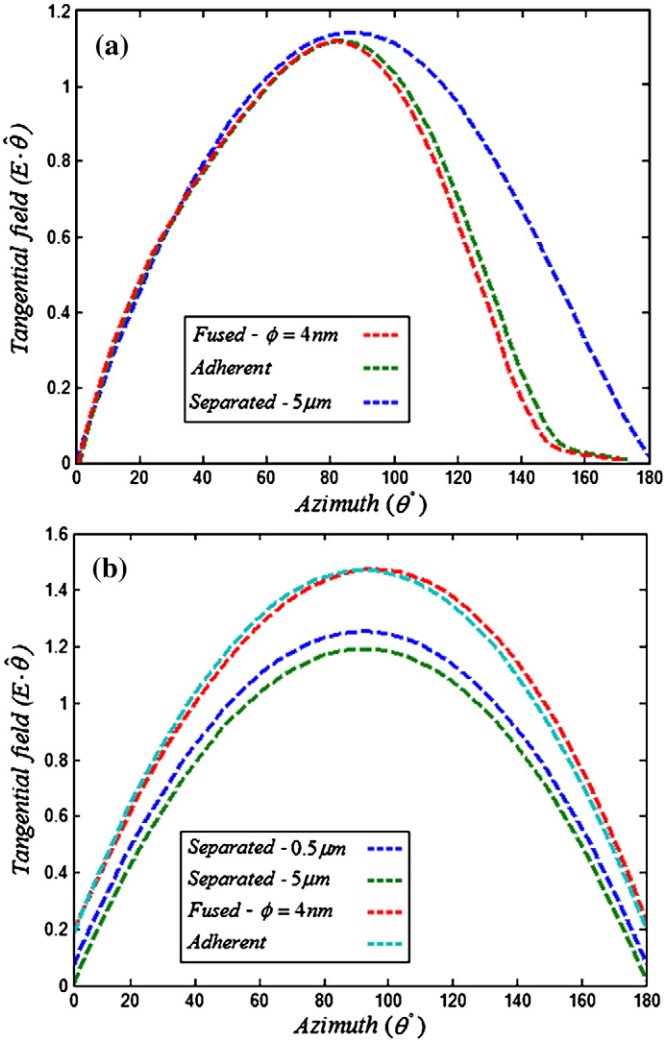

Fig. 10. Tangential membrane field strengths versus the azimuthal angle θ of adhering and fused cells. (a) Membrane field strengths of adhering and fused cells in the parallel orientation as function of separation distance and gap diameter. (b) Membrane field strengths of adhering and fused cells in the perpendicular orientation as function of separation distance and gap diameter.

comparison to the adherent curve. It therefore reinforces the previous finding about the insignificant contribution of the gap.

The obtained differences between the two orientations can be well distinguished by the field and potential maps of fused aggregate given by Fig. 11. At the parallel orientation, at low frequency (~100 Hz), the highly polarized membrane screened the external field within the cytoplasm. At this point, current penetration through the aggregate membrane is quite negligible and the aggregate interior tends to remain nearly equipotential. When the frequency becomes higher (~10 kHz), the current flowing through the gap is increasing, and a potential gradient is observed between its two ends resulting in dispersion event. When the frequency approaches the inverse *R–C* (resistor-capacitor) time of the membrane–medium interface (~3 MHz), current penetration into the cell occurs resulting in dispersion of the membrane. When the frequency becomes much higher (~100 MHz) the potential distribution is governed only by pure dielectric differences between the cytoplasm and the external medium. At the perpendicular orientation, the aggregate interior tends to remain equipotential up to frequencies of about few MHz. Here, only single dispersion is observed which related to the membrane–medium interface. This observation clearly indicates that in the perpendicular orientation, the interior gap can not fundamentally affect the current and potential distribution within the aggregate. It therefore can be concluded that in this case, differences between adherent and fused aggregates are electrically undistinguished.

Although the TMP and field analyses were implemented using simple aggregate models, they allow gaining useful insights about the nature of interaction between spherical suspended cells. Interaction between adherent cells in parallel direction to the field will mainly induce depolarization of the membranes. At this case, the net polarization and hence the permittivity strength will be severely reduced (Fig. 7a). When the cells are fused, the two poles of the membrane become more hyperpolarized and depolarized respectively. Here, low dispersion event is observed when its magnitude found to be significantly influenced by the gap diameter (Fig. 7c). Interactions at the perpendicular orientation will always involve hyperpolarization of the membranes. At this case, the permittivity strength is found to be consistently growing till a point when the cells are fully adhering (Fig. 7b). The later formation of internal gaps between the cells does not fundamentally contribute to the induced polarization, and hence, can not affect the dielectric characteristics of the suspension.

Important issue which is a direct outcome of the current study is related to the concentration of the suspended cells. According to Section 4.3, the electrical space constant λ can provide useful indication regarding the boundaries of interaction between cells. In the case of spherical cells, λ value which is approximately equal to the radius of the cell was obtained. As mentioned, when the separation between the cells is exceeding the electrical space constant ($x>\lambda$), the interactions are getting weaker and the dispersion characteristics are getting fixed. It therefore means that under those conditions the obtained permittivity spectrum is unrestricted by cellular interactions.

From practical point of view and based on the above, the optimal concentration of spherical suspended cells P can be determined based on the calculated λ value. For a spherical cell with radius R and electrical constant λ, the optimal concentration is given by $P \leq R^3/(R+\lambda)^3$. At this case, a theoretical uniform arrangement of cells can be assumed when each cell is surrounded by a spherical sheath with radius of $R+\lambda$. Here, the surrounded medium around each cell is assumed to be cell free. For example, at the current study for $R=2.5$ μm and $\lambda=2.3$ μm a theoretical volume fraction of 0.14 is achieved. This value is found to be in an excellent agreement with previous observations [17,24,31]. Although the λ value was calculated numerically, finite and closed analytical expressions have been elaborated by several authors [12,13] and can be usefully used.

6. Conclusions

In the framework of the study, theoretical examination of the effect of aggregation on the dielectric characteristics of spherical cellular suspension was presented. The dispersion characteristics of several aggregates–cells mixtures have been determined as function of aggregates shape and concentration. In addition, using simple models of adherent and fused cells, quantitative analyses of the cellular interaction between pair of cells was presented. Based on the given analyses, interactions between cells induced significant changes on the polarization state of the lipid membranes, and hence, directly affect the induced dipoles of the interacted cells. Those changes are greatly influenced by the both the orientation and the structural characteristics of the clusters.

The main realizations of the study should mainly be directed to the more practical aspect of cells spectroscopy. Flocculation and aggregation of cells which usually take place under true physiological conditions can greatly affect on the probed properties of cellular suspensions. In this case, both the permittivity spectrum and characteristics will be severely affected, and hence, will not truly represent the characteristics of the suspended fraction. Since the behaviour of most cell types in suspension can not be predicated, the neglect of cell interactions can be quite problematic in most cases and should be carefully considered. Therefore,

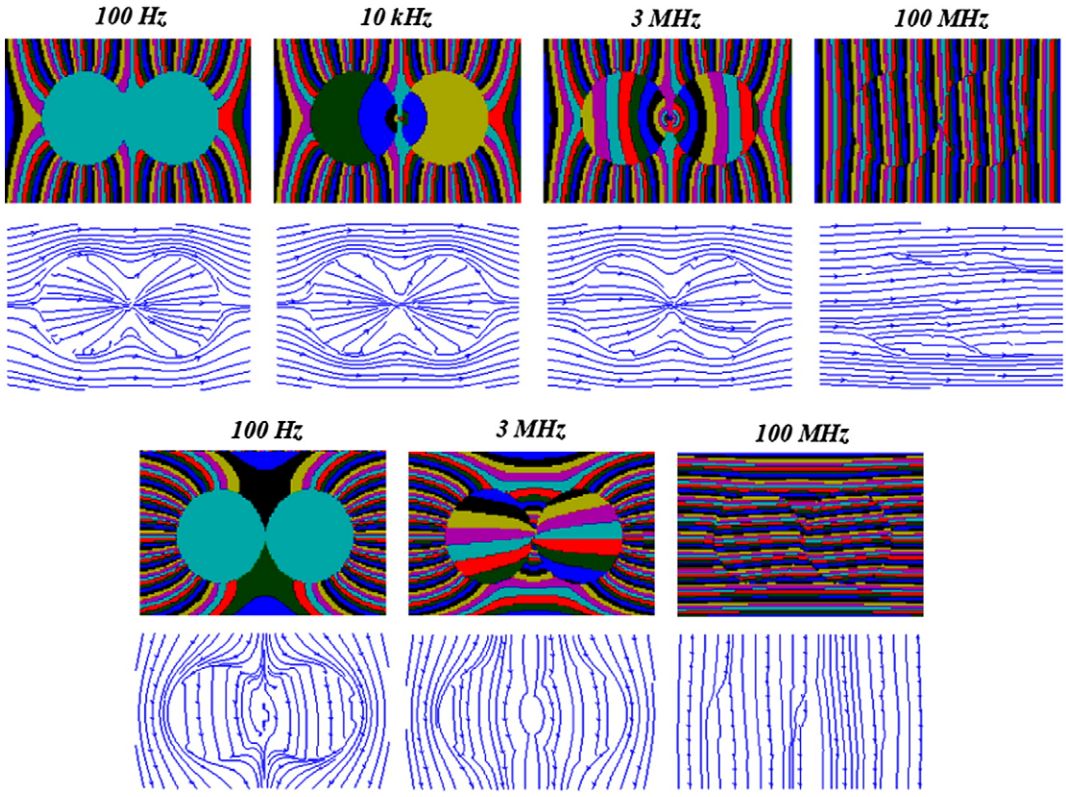

Fig. 11. Cross section of potential and field maps as function of excitation frequency. Upper view: fused cells (ϕ=4 nm) in the parallel orientation. Lower view: fused cells (ϕ=4 nm) in the perpendicular orientation.

and especially in the case of adherent cell lines, pre analysis of the suspended fraction is essential in order to avoid radical formation of cell clusters.

Although the study deals with theoretical examination of aggregation, it can provide important insights into the nature of electrical interactions between cells and their relative effect on the dielectric characteristics of cellular suspensions. However, and without casting doubt on the given analyses, the presented findings must be further examined in tight comparison to true measured characteristics of cellular suspensions. In this case, the aggregation effect should be carefully examined using controlled suspensions which contain different aggregate appearances. Those examinations, combined with finite numerical tools, will allow gaining reliable realizations about the native effect of aggregates when formed in cellular suspensions.

Acknowledgments

The authors would like to thank Dr. Danny Porath for the inspiration behind this work.

Appendix A. Fundamentals of BEM

The boundary element method (BEM) was originally developed for solving the Laplace equation in the late 1970s by Brebbia [20]. The advantages of BEM in comparison to the other numerical methods are best demonstrated on problems governed by the Laplace equation, where the domain problem is transformed into a boundary problem. The boundary is approximated by N elements and the overall solution is constructed based on the superposition of the fundamental solution of each boundary element. The BEM is not restricted to any underlying grid and can take full advantage of the sub pixel accuracy of the boundaries; therefore, it outperforms most of the finite difference approaches.

For an approximate boundary element solution of Laplace equation ($\nabla^2 u=0$) the weighted residual formulation is first applied.

$$\int_R (\nabla^2 u) u^* dR = -\int_{\Gamma_1} (u-\overline{u}) q^* d\Gamma + \int_{\Gamma_2} (q-\overline{q}) u^* d\Gamma \tag{1A}$$

where R is the spatial domain, Γ_1, Γ_2 are complementary portions of the total exterior surface, u is the approximated solutions, $q=\partial u/\partial n$, u^* is the weighting function and $q^*=\partial u^*/\partial n$. Applying Green's theorem twice yields:

$$\int_R (\nabla^2 u^*) u dR = \int_\Gamma (uq^* - qu^*) d\Gamma \tag{2A}$$

When choosing u^* as the fundamental solution of Laplace equation cantered at r' where $\nabla^2 u^* = \delta(\overline{r})$ and $\overline{r} = ||r-r'||$, Eq. (2A) becomes:

$$c_l u = \int_\Gamma (uq^* - qu^*) d\Gamma \tag{3A}$$

where the fundamental solution in two and three dimensions is given by $u^* = -\frac{1}{2\pi}\ln r$ and $u^* = \frac{1}{4\pi r}$ respectively, $c_l=0$ if $r \in (R \cup \Gamma)^c$, $c_l=0.5$ if $r \in \Gamma$ and $c_l=1$ otherwise.

The boundary Γ can be approximated by N boundary elements when u^* and q^* are constant for each element. Eq. (3A) can now be rewritten:

$$c_l u_i = \sum_{j=1}^{N} q_j G_{ij} - \sum_{j=1}^{N} u_j H_{ij} \tag{4A}$$

where $G_{ij} = \int_\Gamma u^* d\Gamma$ and $H_{ij} = \int_\Gamma q^* d\Gamma$, both integrals can be computed analytically for both two-dimensional and three-dimensional problems [20,32].

Appendix B. Supplementary data

Supplementary data associated with this article can be found, in the online version, at doi:10.1016/j.bpc.2008.11.008.

References

[1] J.G. Edwards, J.A. Campbell, The aggregation of trypsinized BHK21 cells, J. Cell Sci. 8 (1971) 53–71.
[2] J.J. Cassiman, M.R. Bernfield, Transformation-induced alterations in fibroblast adhesion: masking by trypsin, Exp. Cell Res. 91 (1975) 31–35.
[3] J.M. Lackie, The aggregation of rabbit polymorphonuclear leucocytes: effects of antimitotic agents, cyclic nucleotides and methyl xanthines, J. Cell Sci. 16 (1974) 167–180.
[4] I.K. Buckley, Three dimensional fine structure of cultured cells: possible implications for subcellular motility, Tissue Cell 7 (1975) 51–72.
[5] M.W. Moosekeh, L.G. Tilney, Organization of an actin filament–membrane complex. Filament polarity and membrane attachment in the microvilli of intestinal epithelial cells, J. Cell Biol. 67 (1975) 725–743.
[6] C.W. Lloyd, D.A. Rees, C.G. Smith, F.J. Judge, Mechanisms of cell adhesion: early forming junctions between aggregating fibroblasts, J. Cell Sci. 23 (1976) 671–684.
[7] J.E.M. Heaysman, S.M. Pegrum, Early contacts between fibroblasts: an ultrastructural study, Exp. Cell Res. 78 (1973) 71–78.
[8] R. Johnson, M. Hammer, J. Sheridan, J.P. Revel, Gap junction formation between aggregated novikoff hepatoma cells, Proc. Natl. Acad. Sci. U. S. A. 71 (1974) 4536–4540.
[9] M.V.L. Bennett, V.K. Verselis, Biophysics of gap junctions, Semin. Cell Biol. 3 (1992) 29–47.
[10] H.P. Schwan, Nonthermal cellular effects of electromagnetic fields: AC-field induced ponderomotoric forces, Br. J. Cancer 45 (1982) 220–224.
[11] A.E. Sowers, Membrane electrofusion: a paradigm for study of membrane fusion mechanisms, Meth. Enzymol. 220 (1993) 196–211.
[12] M.S. Cooper, Gap junctions increase the sensitivity of tissue cells to exogenous electric fields, J. Theor. Biol. 111 (1984) 123–130.
[13] E.C. Fear, M.A. Stuchly, Modeling assemblies of biological cells exposed to electric fields, IEEE Trans. Biomed. Eng. 45 (1998) 1259–1271.
[14] A. Pribush, H.J. Meiselman, D. Meyerstein, N. Meyerstein, Dielectric approach to the investigation of erythrocyte aggregation: I. Experimental basis of the method, Biorheology 36 (1999) 411–423.
[15] K. Asami, K. Sekine, Dielectric modelling of erythrocyte aggregation in blood, J. Phys. D: Appl. Phys. 40 (2007) 2197–2204.
[16] K.R. Foster, H.P. Schwan, Dielectric properties of tissues and biological materials: a critical review, Crit. Rev. Biomed. Eng. 17 (1989) 25–104.
[17] L.K.H. van Beek, Dielectric behaviour of heterogeneous systems, Prog. Dielectr. 7 (1967) 69–117.
[18] S. Takashima, H.P. Schwan, Alignment of microscopic particles in electric fields and its biological implications, Biophys. J. 47 (1985) 513–518.
[19] E. Tuncer, M.G. Stanisław, Dielectric relaxation in dielectric mixtures: Application of the finite element method and its comparison with dielectric mixture formulas, J. Appl. Phys. 89 (2001) 8092–8100.
[20] C.A. Brebbia, The Boundary Element Method for engineers, Pentech press, London, 1978.
[21] O. Alvarez, M. Brodwick, R. Latorre, A. Mclaughlin, S. Mclaughlin, G. Szabo, Large divalent cations and electrostatic potentials adjacent to membranes, Biophys. J. 44 (1983) 333–342.
[22] I. Erimolina, Y. Polevaya, Y. Feldman, Analysis of dielectric spectra of Eukariotic cells by computer modelling, Eur. Biophys. J. 29 (2000) 141–145.
[23] O. Axelsson, Iterative solution methods, Cambridge University Press, 1994.
[24] K. Asami, Characterization of heterogeneous systems by dielectric spectroscopy, Prog. Polym. Sci. 27 (2002) 1617–1659.
[25] E. Tuncer, Y.V. Serdyuk, S.M. Gubanski, Dielectric mixtures: Electrical properties and modelling, IEEE Trans. Electr. Insul. 9 (2002) 809–828.
[26] B. Sareni, L. Krahenbuhl, A. Beroual, Effective dielectric constant of random composite materials, J. Appl. Phys. 81 (1997) 2375–2383.
[27] R.J. Sheppard, The least-squares analysis of complex weighted data with dielectric application, J. Phys. D: Appl. Phys. 6 (1973) 790–794.
[28] J. Bao, C.C. Davis, R.E. Schmukler, Impedance spectroscopy of human Erythrocytes: system calibration and nonlinear modelling, IEEE Trans. Biomed. Eng. 40 (1993) 364–378.
[29] G. Schwarz, M. Saito, H.P. Schwan, On the orientation of nonspherical particles in an alternating electrical field, J. Chem. Phys. 43 (1965) 3562:3569.
[30] K.S. Cole, R.H. Cole, Dispersion and absorption in dielectrics. I. Alternating current characteristics, J. Chem. Phys. 9 (1941) 341–351.
[31] H. Pauly, H.P. Schwan, Uber die Impedanz einer suspension von kugelformigen teilchen mit einer schale, Z. Naturforsch. 14 (1959) 125–131.
[32] T. Kuwabara, T. Takada, Boundary Element Method using analytical integration for Three-Dimensional Laplace problem, Electr. Eng. Jpn. 106 (1986) 530–536.